

Stationary solutions of the one-dimensional nonlinear Schrödinger equation: II. Case of attractive nonlinearity

L.D. Carr^{1*}, Charles W. Clark², W.P. Reinhardt^{1,2,3}

¹*Department of Physics, University of Washington, Seattle, WA 98195-1700, USA*

²*Electron and Optical Physics Division, National Institute of Standards and Technology, Technology Administration, US Department of Commerce, Gaithersburg, MD 20899, USA*

³*Department of Chemistry, University of Washington, Seattle, WA 98195-1700, USA*
(May 19, 2019)

In this second of two papers, we present all stationary solutions of the nonlinear Schrödinger equation with box or periodic boundary conditions for the case of attractive nonlinearity. The companion paper has treated the case of repulsive nonlinearity. Our solutions take the form of stationary trains of bright solitons. Under box boundary conditions the solutions are the bounded analog of bright solitons on the infinite line, and are in one-to-one correspondence with particle-in-a-box solutions to the linear Schrödinger equation. Under periodic boundary conditions we find several classes of solutions: constant amplitude solutions corresponding to boosts of the condensate; the nonlinear version of the well-known particle-on-a-ring solutions in linear quantum mechanics; nodeless, real solutions; and a novel class of intrinsically complex, nodeless solutions. The set of such solutions on the ring are described by the C_n character tables from the theory of point groups. We make experimental predictions about the form of the ground state and modulational instability. We show that, though this is the analog of some of the simplest problems in linear quantum mechanics, nonlinearity introduces new and surprising phenomena in the stationary one-dimensional nonlinear Schrödinger equation. We also note that in various limits the spectrum of the nonlinear Schrödinger equation reduces to that of the box, the Rydberg, and the harmonic oscillator, the latter being for repulsive nonlinearity, thus including the three most common and important cases of linear quantum mechanics.

I. INTRODUCTION

In a recent experiment the dilute-gas, attractive, Bose-Einstein condensate (BEC) was created for the first time for lithium¹⁻³. As predicted by the nonlinear Schrödinger^{4,5} equation (NLSE) for three dimensions⁶, the condensate collapsed when the number of particles became large. However, in one dimension no collapse is predicted, and in one dimension the NLSE has wide application in fiber optics⁷ as well as other fields⁸⁻¹⁰.

In this article we present stationary solutions to the one-dimensional NLSE for attractive nonlinearity under periodic and box boundary conditions. In the preceding article¹¹ we solved the analogous problem for repulsive

nonlinearity. We will place our results in the context of attractive atomic interactions in the BEC.

The BEC is pseudo-one-dimensional when the following criteria are satisfied: $L_y, L_z \lesssim \xi$ and $L_y, L_z \ll L$. Under these criteria the condensate is well out of the Thomas-Fermi limit; i.e. the kinetic energy in the transverse dimensions is very high. It is this high kinetic energy which prevents the condensate from collapsing. As was shown in the previous article¹¹, in pseudo-1D the dimensionless NLSE may be written:

$$[-\lambda^2 \partial_{\tilde{x}}^2 - |f(\tilde{x})|^2 + \tilde{V}(\tilde{x})] f(\tilde{x}) = \tilde{\mu} f(\tilde{x}) \quad (1)$$

where $f(\tilde{x})$ is the dimensionless wavefunction describing excitations along L , $\tilde{x} \in [0, 1]$, $\tilde{V}(\tilde{x})$ is a dimensionless potential representing the boundary conditions, $\tilde{\mu} \equiv (2m\xi^2/\hbar^2)\mu$, and $\lambda \equiv \xi/L$, the ratio of the healing length to the box/ring length. We remind the reader that $\xi^2 \equiv 1/(8\pi\rho|a|)$, where a is the scattering length and ρ is the mean particle density.

For comparison with experiment we list the conversion factor from the unitless $\tilde{\mu}$ to μ in μK . Using the formula from the previous article¹¹, for ^7Li with $\rho = 10^{14}\text{cm}^{-3}$ and $a = -1.45\text{ nm}$, the conversion factor is 0.172. Since the unitless chemical potentials we find will be on the order of 1 to 10 this gives a sense of the energy scale of the solutions, on the order of 0.1 to 1.0 μK . We also note that throughout our presentation we will use a reasonable test scale of $\lambda = 1/25$ for illustrative purposes.

We require the normalization condition:

$$\int_0^1 d\tilde{x} |f(\tilde{x})|^2 = 1 \quad (2)$$

be satisfied together with the NLSE (1) and such boundary conditions as we will describe below. These are the equations we will solve.

II. BOX BOUNDARY CONDITIONS

The key concept underpinning the approach taken in this paper is that in a region of constant potential the NLSE is integrable. This was utilized in our companion paper¹¹, and virtually all the techniques applied there to the case of repulsive nonlinearity apply here as well,

though they lead to the identification of different particular solutions.

Specifically, it was shown in the previous article¹¹ that solutions of the stationary NLSE on the unit interval, subject to the box boundary conditions

$$f(0) = f(1) = 0 \quad (3)$$

can be expressed, without loss of generality, by purely real functions. Such solutions are given in terms of Jacobian elliptic functions, whose properties were reviewed in the previous article. This result holds independent of the sign of the nonlinearity. For the case of repulsive nonlinearity, it was established that the sn function provides all possible solutions. For the attractive case, both the cn and dn functions offer solutions. However, the dn function has no real zeros, so the cn function provides all solutions which satisfy box boundary conditions.

A. Solutions and spectra

The most general form of the solution is:

$$f(\tilde{x}) = A \text{cn}(k\tilde{x} + \delta \mid m) \quad (4)$$

where $0 \leq m \leq 1$ is the parameter of Jacobian elliptic functions. k and δ will be determined by the boundary conditions below while A and m will be determined by substitution of Eq. (4) into the NLSE and by normalization.

Since the quarter period of cn is the complete elliptic integral of the first kind, $K(m)$, and since $\text{cn}(0 \mid m) = 1$, we find that $k = 2jK(m)$ and $\delta = -K(m)$, where $j \in \{1, 2, 3, \dots\}$. The physical meaning of $j - 1$ is the number of nodes in the cn function. We will give a more general meaning to j below. We then solve Eq. (1) by substituting Eq. (4), using Jacobian elliptic identities, and setting coefficients of equal powers of cn equal. This results in equations for the amplitude squared, A^2 and the chemical potential, $\tilde{\mu}$:

$$A^2 = 2m(2jK(m))^2 \lambda^2 \quad (5)$$

$$\tilde{\mu} = -(2jK(m))^2 \lambda^2 (2m - 1) \quad (6)$$

Substituting Eq. (5) into Eq. (2), utilizing Jacobian elliptic identities, and noting that the integral over cn^2 can be defined in multiples of the quarter period $K(m)$, we obtain the normalization condition:

$$2(2j)^2 \lambda^2 K(m) (E(m) - (1 - m)K(m)) = 1 \quad (7)$$

where $E(m)$ is the complete elliptic integral of the second kind. Eq. (4) then becomes:

$$f(\tilde{x}) = \sqrt{2m}(2jK(m))\lambda \text{cn}(K(m)(2j\tilde{x} - 1) \mid m) \quad (8)$$

This leaves the chemical potential (6) and the wavefunction (8) determined up to the parameter m and the

scale λ . In Fig. 1 a graphical solution of Eq. (7) is shown. The plot demonstrates that the solution is unique. Note that the normalization condition requires m to be much closer to 1 than in the repulsive case, as may be seen by comparing Fig. 1 to the corresponding figure in the previous article¹¹. It follows that the numerics of the attractive case are more difficult than those of the repulsive one.

These solutions are in one-to-one correspondence with those of the 1D particle-in-a-box problem in linear quantum mechanics. Plots of the wavefunction for the first three energy levels and a highly excited state are shown in Fig. 2. Low-lying states are characterized by distinct amplitude peaks. The widths of these peaks increase as their separations decrease, or as they approach the wall of the box. Physically, the kinetic energy tends to spread out the peaks. Note that if the wavefunction is squared to give the single particle density then the density is exponentially small everywhere except at the peaks.

In Fig. 3 we plot the chemical potential spectrum of this solution type as a function of λ^{-2} , the number of healing lengths per box length quantity squared. Note that in comparison to the repulsive case the spectrum in this and following plots are less smooth. In fact the numerics are difficult in the repulsive case as well. It is simply that the smooth, limiting expressions sufficed for the whole of the plot in the repulsive case, while here we had to calculate the chemical potentials point by point.

The leftmost portion of the plot corresponds to the particle-in-a-box limit and the rightmost portion to the bright soliton limit. We now discuss these two limits.

B. Particle-in-a-box limit

High chemical potential states in which the peaks overlap become particle-in-a-box type solutions, as can be seen in Fig. 2d. This is both the zero density, linear limit and the highly-excited-state limit. Mathematically, $m \rightarrow 0^+$ and $\text{cn} \rightarrow \cos$. Physically, $j\lambda \gg 1$. In this limit $K(m) \rightarrow \pi(1/2 + m/8 + \mathcal{O}(m^2))$ and $m \rightarrow 1/(j\pi\lambda)^2$, so that Eq. (6) becomes:

$$\begin{aligned} \tilde{\mu} &= j^2 \pi^2 \lambda^2 \left(1 - \frac{3m}{2} + \mathcal{O}(m^2)\right) \\ \tilde{\mu} &= j^2 \pi^2 \lambda^2 \left(1 - \frac{3}{2j^2 \pi^2 \lambda^2} + \mathcal{O}\left(\frac{1}{j^4 \lambda^4}\right)\right) \end{aligned} \quad (9)$$

or putting back in the units:

$$\begin{aligned} \mu &= \frac{j^2 \pi^2 \hbar^2}{2ML^2} \left(1 - \frac{3m}{2} + \mathcal{O}(m^2)\right) \\ \mu &= \frac{j^2 \pi^2 \hbar^2}{2ML^2} \left(1 - \frac{12aNL}{A_t j^2 \pi} + \mathcal{O}\left(\frac{L^2 N^2}{j^4}\right)\right) \end{aligned} \quad (10)$$

which clearly converges to the well-known linear quantum mechanics particle-in-a-box chemical potential. Note

that the first order correction is identical to the repulsive case except that it is negative. One may also obtain this result from first order perturbation theory, as has been shown in the previous article¹¹.

C. Bright soliton limit

One may add a peak without disturbing another peak, provided that adjacent peaks have opposite phase and that the overlap between them is exponentially small in the ratio of their separation to their healing length. In this limit we ought to recover a series of equally spaced sech solutions of alternating phase to within exponentially small factors, as for example is shown in Fig. 2b and Fig. 2c. Sech solutions are also called bright solitons. The sech function is the $m \rightarrow 1^-$ limit of the cn function in the solution, Eq. (4).

Bright solitons solve the NLSE with zero potential. Thus we should find that the wavefunction and chemical potential no longer depend on the box length L . In this limit the solitons must have a different length scale than λ , which depended on L . The soliton width is proportional to the parameter

$$\eta \equiv \frac{A_t}{8\pi N |a|}, \quad (11)$$

where A_t is the transverse area of the box. In the soliton literature⁷, η is usually set to 1 by renormalizing the wavefunction.

We now consider the limit $\lambda \rightarrow 0$, which corresponds to $m \rightarrow 1^-$. Physically, this means that the peaks become highly separated and the interaction between them becomes exponentially small. By using Taylor expansions in $(1 - m)$ of the complete elliptic integrals in Eq. (7) we find that Eq. (6) becomes:

$$\tilde{\mu} = -\frac{1}{16j^2\lambda^2} \quad (12)$$

while Eq. (8) becomes:

$$f(\tilde{x}) = \frac{1}{2^{3/2}j} \lambda^{-1} \text{cn}\left(\frac{1}{8j^2\lambda^2}(2j\tilde{x} - 1) \mid m\right) \quad (13)$$

Putting back in the units we find:

$$\mu = -\frac{\hbar^2}{2m} \frac{1}{16\eta^2} \frac{1}{j^2} \quad (14)$$

$$\frac{f(x)}{\sqrt{L}} = \frac{1}{2^{3/2}j} \frac{1}{\eta} \text{cn}\left(\left(\frac{1}{4j\eta}\right)x - \delta(L) \mid m\right) \quad (15)$$

where $\delta(L)$ is an offset which depends on the box length. But as $L \rightarrow \infty$ the offset becomes arbitrary, so that we can set it to zero. Note that we put back in the units of the wavefunction $f(x)$ which we took out in making the

separation of variables in the pseudo-1D approximation. Eq. (14) is identical in form to that of the Rydberg for the Hydrogenic atom.

As the reader may verify, for the case in which $j = 1$ this is indeed the chemical potential and wavefunction of the sech solution to the free 1D NLSE:

$$\frac{f(x)}{\sqrt{L}} = \frac{1}{2^{3/2}} \frac{1}{\eta} \text{sech}\left[\left(\frac{1}{4\eta}\right)x \mid m\right] \quad (16)$$

We have found that this limit suffices to calculate chemical potentials for which $j < 1/(5\lambda)$ to better than 1%. This estimate assumes an overall scale size of $\sim 5\xi$ per kink. The L -independent chemical potentials for the $j=1$, $j=2$, and $j=3$ solutions shown in Fig. 2 satisfy this criterion, for example, as do any ground states for a healing length smaller than $1/10$.

III. PERIODIC BOUNDARY CONDITIONS

There are four solution types for periodic boundary conditions. There are constant amplitude solutions which are plane waves; real, antisymmetric, symmetry-breaking solutions, similar to those found in Sec. II; real, symmetric, symmetry-breaking solutions; and a novel class of complex symmetry-breaking solutions. The former two are in one-to-one correspondence with particle-on-a-ring solutions in linear quantum mechanics, while the latter two are only found in the presence of nonlinearity. As the ring is rotationally invariant, the symmetry-breaking solutions will have a high degeneracy, in analogy with vortices in two dimensions²³. The periodic boundary conditions are:

$$f(0) = f(1) \quad (17)$$

$$f'(0) = f'(1) \quad (18)$$

A. Constant amplitude solutions

If we assume that $r(\tilde{x}) = \text{constant}$ then we obtain constant amplitude solutions of the form:

$$f(\tilde{x}) = e^{i2\pi n\tilde{x}} \quad (19)$$

where $n \in \{0, \pm 1, \pm 2, \dots\}$. The amplitude is constrained by normalization to be 1. Substituting Eq. (19) into Eq. (1) we find the chemical potential:

$$\tilde{\mu} = -1 + (\lambda 2\pi n)^2 \quad (20)$$

Unlike for the case of repulsive nonlinearity, where the ground state on a ring was the constant solution for $n = 0$, the attractive BEC prefers to clump into peaks, so that the constant amplitude solutions are a highly excited states for most scales. This will be discussed further in Sec. V A. Note that for $n \neq 0$ each solution is two-fold degenerate, as n can be either positive or negative.

B. Real symmetry-breaking solutions

Of the two Jacobian elliptic functions having different physical form and solving the NLSE for attractive nonlinearity, only one could be used for the box, the cn function. The dn function satisfied the NLSE but, as it never vanished, failed to satisfy box boundary conditions. But on the ring the dn function poses no difficulty, because the boundary conditions are periodic. Thus two real solution types are available. Looking at the plot of the Jacobian elliptic functions in the appendix to the previous article¹¹, we observe that the cn function is anti-symmetric with respect to translation by the half period $2K(m)$, while the dn function is symmetric under such a translation.

1. Analog to box boundary condition solutions

As we have exchanged the ring for the box, Eq. (4) is the real solution. One simply changes k from $2jK(m)$ to $4jK(m)$ in order to satisfy Eqs. (17) and (18), i.e. from multiples of the half period to multiples of the whole period. The number of nodes will be $2j$ rather than $j-1$, where $j \in \{1, 2, 3, \dots\}$. We temporarily keep δ set to 0. But note that, unlike for box boundary conditions, under periodic boundary conditions δ is arbitrary.

Then all the results from section II hold with the new k , by letting $j \rightarrow 2j$ in all equations. The energy and wavefunction are determined uniquely by graphical solution of Fig. 1. In Fig. 4 we show the first few states and a highly excited state. Both the linear quantum mechanics, particle-on-a-ring limit and the bright soliton limits are reproduced. In the latter the same kind of non-overlapping criterion applies as before.

We found real solutions by setting $\delta = 0$. If we instead let δ vary arbitrarily, we obtain the degeneracy inherent in these symmetry-breaking solutions. The entropy associated with a pair of peaks depends logarithmically on the box length L , and, since there are approximately λ^{-1} possible positions for a peak, the entropy is^{11,23}:

$$S \sim k_B \ln\left(\frac{1}{10j\lambda}\right) \quad (21)$$

where the factor of 10 comes from 5 for each of the two peaks. This is consistent with the non-overlapping criterion used in obtaining Eq. (14).

2. Nodeless solutions

To find the dn solutions, we follow the same method as outlined in Sec. II. The most general solution is:

$$f(\tilde{x}) = A \operatorname{dn}(k\tilde{x} + \delta | m) \quad (22)$$

subject to the NLSE (1), the normalization (2), and the boundary conditions (17) and (18). From these we obtain the chemical potential, normalization, and amplitude:

$$\tilde{\mu} = -(2jK(m))^2 \lambda^2 (2 - m) \quad (23)$$

$$2(2j)^2 \lambda^2 K(m) E(m) = 1 \quad (24)$$

$$f(\tilde{x}) = \sqrt{2}(2jK(m)) \lambda \operatorname{dn}(K(m)(2j\tilde{x} - 1) | m) \quad (25)$$

where j refers to the number of peaks rather than nodes in the dn function, since the dn function is nodeless. Note that Eqs. (23)-(25) are only valid for $m \neq 0$. The $m = 0$ case is discussed in Sec. III D.

The dn function has a period of $2K(m)$, not $4K(m)$ as did the cn function. Plots of the amplitude for the first three energy levels and a higher excited state are shown in Fig. 5. We have plotted a $j = 5$ excited state rather than a $j = 10$ because there are no solutions at this scale above $j = 5$, as we shall make clear in Sec. III D.

The ground state, shown in Fig. 5a, appears identical to the ground state shown in Fig. 2a. Because m is very close to 1 for the test scale of $\lambda = 1/25$, $\operatorname{dn} \sim \operatorname{sech}$ and $\operatorname{cn} \sim \operatorname{sech}$, so that $\operatorname{cn} \sim \operatorname{dn}$. Had we chosen a scale at which the peaks came near to the boundaries, the two ground state solutions would have looked quite different. To make clear the extent to which m is singular at this scale, the numerical solution to Eq. (24) for a single peak is $(1 - m) \simeq O(10^{-66})$.

The particle-on-a-ring limit for the dn solution is a plane wave. As $m \rightarrow 0^+$, $\operatorname{dn} \rightarrow 1$. In this case the amplitude is constrained to be 1 by the normalization and the chemical potential is $\tilde{\mu} = -1$.

In the bright soliton limit Eq. (24) may be expanded in $(1 - m)$ to yield the same result for the chemical potential and amplitude as was found for the cn solutions in a box:

$$\mu = -\frac{\hbar^2}{2m} \frac{1}{16j^2} \frac{1}{\eta^2} \quad (26)$$

$$\frac{f(x)}{\sqrt{L}} = \frac{1}{2^{3/2}j} \frac{1}{\eta} \operatorname{dn}\left(\left(\frac{1}{4j\eta}\right)x - \delta(L) | m\right) \quad (27)$$

where the same criterion as was used for the cn solutions in a box may be applied to the validity of the use of the limit here.

As with the cn solutions, we found the nodeless dn solutions by setting $\delta = 0$. If we instead let δ vary arbitrarily, we obtain the degeneracy inherent in these symmetry-breaking solutions. The entropy associated with a peak depends logarithmically on the box length L , and, since there are approximately λ^{-1} possible positions for a peak, the entropy is:

$$S \sim k_B \ln\left(\frac{1}{\pi\sqrt{2}j\lambda}\right) \quad (28)$$

where the factor of $\pi\sqrt{2}$ will be explained in Sec. III D.

3. Energy splittings

Because the dn solutions are symmetric and the cn solutions are anti-symmetric, we expect that for even numbers of peaks the chemical potentials of the two solution types should be very close. For odd numbers of peaks there are no cn solutions.

Removing all factors in common to the two chemical potentials we find from Eq. (6) and Eq. (7) for the cn solution and from Eq. (23) and Eq. (24) for the dn solution:

$$\tilde{\mu}_{\text{cn}}(m_{\text{cn}}) \propto -\frac{2m_{\text{cn}} - 1}{E[m_{\text{cn}}] - (1 - m_{\text{cn}})K[m_{\text{cn}}]} \quad (29)$$

$$\tilde{\mu}_{\text{dn}}(m_{\text{dn}}) \propto -\frac{2 - m_{\text{dn}}}{E[m_{\text{dn}}]} \quad (30)$$

where m_{cn} is found by solving Eq. (7) numerically and m_{dn} is found by solving Eq. (24) numerically. This gives the exact percent splitting:

$$\%_{\text{split}} = 100 \frac{\tilde{\mu}_{\text{dn}}(m_{\text{dn}}) - \tilde{\mu}_{\text{cn}}(m_{\text{cn}})}{\frac{1}{2} |\tilde{\mu}_{\text{dn}}(m_{\text{dn}}) + \tilde{\mu}_{\text{cn}}(m_{\text{cn}})|} \quad (31)$$

In Fig. 6 we show the $m_{\text{cn}} \rightarrow 1^-$ and $m_{\text{dn}} \rightarrow 1^-$ limit of $\%_{\text{split}}$. In this limit $m_{\text{cn}} \sim m_{\text{dn}}$. The small noisy region on the plot between $-\log(1 - m) = 0$ and $-\log(1 - m) = 1$, i.e. between $m = 0$ and $m = 0.9$, is simply where the approximation $m_{\text{cn}} \sim m_{\text{dn}}$ has broken down. In this region we have checked numerically and have found that the splitting can be as high as 30% and is highly scale dependent. We shall discuss the scale dependence further in Sec. VB, as we must first know something about bounds. However, both in the limit we show in Fig. 6 and in the region we examined numerically the dn solution is always higher in chemical potential than the cn solution.

In linear quantum mechanics it is known that for the spatial wavefunctions of two particles the antisymmetric superposition is higher in energy than the symmetric superposition. Qualitatively, if the wavefunctions are squared it is easy to see that the antisymmetric probability density is sharper and always goes to zero in the center, whereas the symmetric probability density is smoother and need not go to zero in the center. Thus it costs more energy to make an antisymmetric superposition. The more the wavefunctions overlap, the higher the percent splitting between the two energies.

The exact opposite is true in the NLSE. The symmetric, nodeless, dn solutions are *higher* in chemical potential than the antisymmetric cn solutions. The $m \rightarrow 0^+$ limit in the plot corresponds to the wavefunctions maximally overlapping. Just as in linear quantum mechanics, the more the wavefunctions overlap the higher the splitting.

C. Complex symmetry-breaking solutions

Our treatment is identical to that of the repulsive case¹¹. By the same arguments used there, all intrinsically complex solutions to Eq. (1) may be written as a sum over standard elliptic integrals by the use of appropriate Cayley transformations²².

Writing the wavefunction as:

$$f(\tilde{x}) = r(\tilde{x})e^{i\phi(\tilde{x})} \quad (32)$$

one may divide the NLSE into real and imaginary parts:

$$(S')^2 = -2 \left[-\frac{1}{\lambda^2} S^3 + \frac{2\tilde{\mu}}{\lambda^2} S^2 - \beta S + 2\alpha^2 \right] \quad (33)$$

$$\phi' = \frac{\alpha}{S} \quad (34)$$

where α and β are undetermined constants of integration and $S \equiv r(\tilde{x})^2$ is the single particle density $|f(\tilde{x})|^2$.

From substituting Eq. (32) into Eqs. (17)-(18) and again taking real and imaginary parts, four boundary conditions are obtained, the important one being phase quantization:

$$\phi(1) - \phi(0) = 2\pi n \quad (35)$$

where n is an integer which we will call the phase quantum number.

Thus for the complex solutions, Eq. (33) and Eq. (34) replace the NLSE as the equations to solve, together with four boundary conditions, of which phase quantization is the most important, and the normalization, Eq. (2).

In Secs. IIIB 1 and IIIB 2 we showed that the real symmetry-breaking solutions have a density proportional to cn^2 and dn^2 , respectively. The former of these vanishes at $2j$ points around the ring, while the latter is nodeless. We look for complex solutions which effectively interpolate between these two real solution types. The motivation for such a solution will become clear in Sec. IVA. Using our physical intuition, we are again able to bypass the use of Cayley transformations, as we did in the repulsive case.

We remind the reader of the Jacobian elliptic function identity:

$$\text{cn}^2(\tilde{x} | m) = \frac{1}{m} (\text{dn}^2(\tilde{x} | m) - (1 - m)) \quad (36)$$

We thus generalize the real symmetry-breaking solutions, Eq. (4) and Eq. (22), as follows:

$$r^2(\tilde{x}) = A^2 (\text{dn}^2(k\tilde{x} + \delta | m) - \gamma(1 - m)) \quad (37)$$

When $\gamma = 0$ the dn solution is recovered; when $\gamma = 1$ the cn solution is recovered. As in the repulsive case, we temporarily set $\delta = 0$. j is to be interpreted as the number of peaks in the density $r(\tilde{x})^2$. We will consider the case of general δ , and thus degeneracy, later.

Using the solution methods as outlined in the repulsive case¹¹, k is set to $2jK(m)$ in order to satisfy the boundary conditions. The solution then becomes:

$$r^2(\tilde{x}) = A^2(\text{dn}^2(2jK(m)\tilde{x} \mid m) - \gamma(1 - m)) \quad (38)$$

The chemical potential and the parameters γ , A^2 , and α are then:

$$\tilde{\mu} = -\frac{3}{2} + 12j^2\lambda^2 E(m)K(m) - 4j^2(2 - m)\lambda^2 K(m)^2 \quad (39)$$

$$\gamma = \frac{-j^{-2}\lambda^{-2} + 8E(m)K(m)}{8(1 - m)K(m)^2} \quad (40)$$

$$A^2 = 8j^2\lambda^2 K(m)^2 \quad (41)$$

$$\alpha = \frac{1}{\sqrt{2}} \left[\lambda^{-2}((-1 + 8j^2\lambda^2 E(m)K(m) - 8j^2(1 - m)\lambda^2 K(m)^2) * (1 + 8j^2\lambda^2 K(m)^2 + 64j^4\lambda^4 E(m)^2 K(m)^2 - 16E(m)(j^2\lambda^2 K(m) + 4j^4\lambda^4 K(m)^3))) \right]^{1/2} \quad (42)$$

This leaves the constant of integration α in Eq. (34), the interpolation parameter γ , the prefactor to the density A^2 , and the chemical potential $\tilde{\mu}$, determined up to the number of peaks j , the scale λ , and the parameter m . For a given λ and j we then numerically integrate Eq. (34) and adjust m until the phase is quantized on the ring, i.e. until n is an integer.

All parameters are monotonic in m . Furthermore m has an extremely limited range. Because the solution (38) was designed to interpolate between the two real solution types, outside of the small splitting between the value of m for the real cn and dn solutions (see Sec. IIIA3) there are no complex solutions at all. We find numerically that outside of these splittings α becomes purely imaginary. This would invalidate the hypothesis that the phase is real. Thus to find the complex solutions one need only scan the values of m between m_{cn} and m_{dn} , so that the algorithm is quite straightforward.

If there are an odd number of peaks then there is no cn solution. In this case we just consider the odd-peaked cn solution for the box, and treat it as a limiting case of the complex solutions. By symmetry of the ring, n can be either positive or negative, so that each solution is two-fold degenerate, just as we found for the constant amplitude solutions.

In Fig. 7 we show the amplitude and phase of two solutions at the test scale of $\lambda = 1/25$. We have plotted the amplitude above the phase to make apparent that the phase is nearly constant over the peaks and jumps sharply between them. In Fig. 8 we plot a five-peaked solution of $n = 2$ and its limiting case of $n \rightarrow 2.5^-$, the

latter being the cn-like limit of $\gamma \rightarrow 0^+$. From the two plots we see that when the troughs go to zero, the phase becomes a step function. In the $j = 5$ example there are five peaks and thus five steps. The height of each step approaches π .

The closer the troughs are to zero, the more pronounced the jump. Since the phase is constant over a stationary bright soliton as well its bounded analogue the cn, it follows that it should approach a step function in the cn-like limit. The phase can only change at the nodes. As a consistency check, we note that all of the chemical potentials and other parameters in the complex case approached the values found in the real case as $\gamma \rightarrow 0^+$ and $\gamma \rightarrow 1^-$, respectively.

If we generalize δ so that it is arbitrary, we obtain a similar degeneracy to what we found in Eqs. (21) and (28):

$$S \sim k_B \ln\left(\frac{1}{\pi\sqrt{2}j\lambda}\right) \quad (43)$$

where the factor of $\pi\sqrt{2}$ will be explained in Sec. IIID.

D. Bounds

We set three types of bounds on the complex solutions. The first is a maximum chemical potential. The second is a maximum and minimum phase quantum number n for a given scale λ and number of peaks j . The third is a minimum inverse scale λ^{-1} for j peaks and n phase quanta to be available, where we use inverse scale rather than scale for plotting convenience. Because the real dn solutions are *exactly* reproduced by the complex solution method, rather than being a limiting case, as was true for the cn, the bounds will be equally applicable to both complex and dn solutions types. One can imagine that if there are only five healing lengths around the ring then there will be no nodeless 100 peak solution. All three bounds rely on this idea.

Mathematically we obtain the maximum number of peaks that can fit on the ring from the lower limit on the period of the dn function in the solution (38). When the peaks overlap too much they are no longer solutions to the NLSE. The dn function approaches its minimum period of π as $m \rightarrow 0^+$. In this limit Eq. (39) becomes:

$$\tilde{\mu}_{\text{max}} = -\frac{3}{2} + 2j^2\lambda^2\pi^2 \quad (44)$$

Physically we expect the maximum chemical potential should occur when the peaks overlap maximally. Thus Eq. (44) sets an upper bound on the chemical potential of each j peak, n phase quanta, intrinsically complex solution, the first bound which we mentioned above. In this same limit the amplitude approaches a constant which the normalization constrains to be 1. From Eqs. (34)

and (42) we find a relation between the maximum number of peaks, the phase quantum number, and the scale λ :

$$\lambda = \frac{1}{\pi \sqrt{2j_{max}^2 - 8n^2}} \quad (45)$$

If $n = 0$ we ought to recover the dn solution, as we did in Fig. 7c. Indeed, substituting Eq. (45) into Eq. (44) and setting $n = 0$ we find that $\tilde{\mu}_{max} = -1$. This is the chemical potential of the dn solution which we found in the particle-on-a-ring linear quantum mechanics limit, the constant solution.

We can set a bound on the phase quanta simply from the parameter range mentioned in Sec. IIIC. Because the complex solutions interpolate between the cn and dn solutions:

$$0 \leq n < \frac{j}{2} \quad (46)$$

This is the second bound which we mentioned above. Note that n is strictly less than $j/2$. This is because the phase quanta of the cn solution is actually 0, not $j/2$. $j/2$ is the limiting case, and j can be odd, even though an odd-peaked cn solution does not solve the NLSE on the ring.

The third kind of bound is that for a given λ^{-1} only certain j and n are possible. In Fig. 9 we plot the inverse scale at which each j becomes available for the maximum n within the range of n . For odd j this is only half a phase quantum away from $j/2$, while for even j it is a whole phase quantum away. Thus we expect that the odd j solutions should become available sooner than the even j solutions due to the quantization condition. The precise inverse scale at which j peaks becomes possible is:

$$(\lambda^{-1})_{min} = \pi \sqrt{-8 + 8j_{even}} \quad (47)$$

for even j , and

$$(\lambda^{-1})_{min} = \pi \sqrt{-2 + 4j_{odd}} \quad (48)$$

for odd j .

The order of j -peaked solutions turning on as a function of λ^{-1} can be read off of Fig. 9 as: 1, 2, 3, 5, 4, 7, 9, 6, 11, 13, 8, ... Thus the expectation that odd j solutions are available sooner is fulfilled for $j > 3$. For large λ^{-1} many more odd than even solutions are available, as again may be seen in the plot.

Both in Fig. 9 and in Eqs. (47) and (48) we see that the minimum inverse scale for a complex solution is $\pi\sqrt{2}$. This means that the ground state for less than about 4.5 healing lengths to the box length is the $n = 0$ constant solution, rather than the single-peaked $n = 0$ dn solution. This is also the source of the constant factor in the entropy of the dn and complex solutions, Eqs. (28) and (43). $\pi\sqrt{2}$ is the minimum size of a peak.

Finally we note that while the complex solutions can have both an even and odd number of peaks and never go

to zero, the real cn solutions have only an even number of peaks. Therefore odd j solutions never go to zero, and where even j complex solutions do not exist but odd ones do, as we have shown above is the case for large j , the peak to background ratio will vary greatly from odd to even numbers. To illustrate this, in Fig. 10 we plot the maximal odd j , complex solution of $j = 15$ for the test scale of $\lambda = 1/25$ and an even j , real cn solution of $j = 16$. Note the extreme variance in depth.

Supposing that λ is small there are three regimes. For small j all solution types are available. For intermediate j even-peaked solutions are cn and go to zero, while odd-peaked solutions are complex and shallow. For large j only cn solutions are available, so that there are no odd-peaked solutions.

E. Spectra

The chemical potential $\tilde{\mu}$ is highly dependent on the scale λ . There is no simple ordering of chemical potential levels. As the real solutions are limiting cases of the complex solutions, the two scale in the same way and their levels do not cross. But the constant amplitude solutions depend differently on inverse scale, so their levels can cross with the other solutions.

In Fig. 11, Fig. 12, Fig. 13, and Fig. 14 we show the chemical potential spectra as a function of λ^{-1} for the four solutions types which we have considered: real with nodes, real without nodes, constant amplitude, and intrinsically complex. We have used the same scales for the four plots, so that the reader may compare them. We have plotted over inverse scale squared. This is to highlight the bright soliton limit, for which the chemical potential is proportional to λ^{-2} , as we detail in Sec. IIC. All data was produced following the algorithms detailed above.

Fig. 12 and Fig. 14 are both very linear because they are in the bright soliton regime. As soon as the peaks overlap appreciably these two solution types no longer become available. However, for the cn spectra shown in In Fig. 11 we see that both the bright soliton limit, to the far right, and the particle-in-a-box limit, to the far left, hold.

Looking at Fig. 13 we see that for an inverse scale of less than about 4 the ground state is the $n = 0$, $\tilde{\mu} = -1$ constant amplitude solution, since no other nodeless solution types are available and the cn solutions are quite high in chemical potential. Since this is the particle-on-a-ring regime, we expect the ground state to be a constant.

For the test scale of $1/25$ the ground state is the single-peaked, nodeless dn solution. The first excitation is the two-peaked anti-symmetric cn solution, the second is the two-peaked dn solution, the third is the three-peaked $n = \pm 1$ complex solution, the fourth is the three-peaked dn solution, and so forth, according to the ordering which we layed down in Sec. IIID.

IV. MATHEMATICAL CONNECTIONS

A. Theory of point groups

From Eq. (1) we may consider the negative nonlinear term in the NLSE as an effective potential generated by the wavefunction. As long as the peaks in the wavefunction are well separated then the self-generated dips do not interact. On a ring we may treat the well-separated limit as a rotationally symmetric set of j potential wells, where j is, as before, the number of peaks in the magnitude of the wavefunction. In Fig. 15 we show the case for $j = 5$.

This is in complete analogy to the quantum dynamics of a particle in a j -fold rotationally symmetric potential in two dimensions. Such a physical situation is described by the C_j symmetry point group. The number of irreducible representations of the C_j group determines the degeneracy of the solutions. Thus we may look up the C_j character tables²⁶ in order to find the degeneracy.

In Sec. IIIC we considered the case of $j = 5$. We found a real, $n = 0$, dn solution and two complex solutions for $n = 1$ and $n = 2$. As the two complex solutions were each two-fold degenerate there were 5 solutions in all. This is exactly what we find in the C_5 character table²⁶: there are one real solution and two doubly-degenerate, intrinsically complex solutions. The latter are essentially a linear combination of independent bright solitons with coefficients which are simply the appropriate group characters, as familiar to chemists in molecular orbital theory²⁷.

In the limit that $\lambda \rightarrow 0^+$, i.e. that the peaks are well separated, given j peaks there are j nearly degenerate solutions. If j is even there are 2 real solutions, one symmetric and one antisymmetric, and $(j-2)/2$ complex solutions, each two-fold degenerate. The splitting is given by Eq. (31). If j is odd there is only one real solution, the symmetric one, and $(j-1)/2$ complex solutions, each two-fold degenerate.

An upper bound may be placed on the splitting by applying Eq. (31) and keeping in mind that the odd-peaked cn solution is a limiting case on the ring. For both even and odd j the ordering of the chemical potentials is as detailed in Sec. IIID, with the anti-symmetric solution being the lowest and the other symmetry-breaking solutions being higher in chemical potential as $n \rightarrow 0^+$. There is an additional degeneracy due to symmetry-breaking, as seen in Eqs. (21), (28), and (43).

Thus we have shown by group theoretic considerations that our bright stationary state solutions to the NLSE under periodic boundary conditions include all symmetry-breaking eigenstates of evenly spaced peaks identical up to a phase.

B. Soliton theory

The elementary sech solution is known as a bright soliton. Both the cn and dn functions are sech-like solutions which satisfy the NLSE for periodic boundary conditions and can be considered as bright soliton-trains. In our previous article¹¹ we showed that the intrinsically complex solutions on the ring were the bounded analog of soliton solutions on the infinite line, known as grey solitons, with the condensate given a momentum boost in the opposite direction, so that the solitons were stationary in the lab frame. For repulsive nonlinearity the complex solution was:

$$r^2(\tilde{x}) = A^2(1 + \gamma \text{dn}^2(k\tilde{x} + \delta | m)) \quad (49)$$

which with the condensate boost removed and in the limit as $m \rightarrow 1^-$ became the known grey soliton solutions²⁴:

$$f(x - ct, t) = \sqrt{2} \left[i \frac{c\nu}{2\xi} + \xi \kappa \tanh(\kappa(x - ct)) \right] e^{-i\mu t/\hbar} \quad (50)$$

where κ is the width, c is the speed, and $\nu \equiv 2M\xi^2/\hbar$. However, in the present work no such analog exists. For in the limit as $m \rightarrow 1^-$ the solution (37) only recovers the real sech solution. This is because Eq. (37) interpolates between cn and dn, both of which become a sech on the infinite line.

Therefore, to the authors' knowledge, for *attractive* nonlinearity on a ring we have found an entirely new type of soliton-train solution which has not been explored in any field in which the nonlinear Schrödinger equation is applied. One could imagine searching for such solution types in the Bose-Einstein condensate as well as in fiber optics or other contexts.

V. EXPERIMENTAL PREDICTIONS

A. Formation of the ground state

We showed in Sec. IIID that for $\lambda^{-1} < \sqrt{2}\pi$ the lowest chemical potential solution on the ring is a constant. There is no longer a single peaked solution. Instead the first excited state is the two-peaked cn solution. As λ^{-1} is increased a broad single-peaked solution becomes available which is lower in chemical potential than the constant solution. For further increase in λ^{-1} the width of the peak becomes steadily smaller and the chemical potential decreases.

The regime in which the kinetic energy entirely dominates over the mean field energy is defined by $\lambda^{-1} < \sqrt{2}\pi$. As defined in Sec. I, ξ^2 is inversely proportional to the number of particles and to the scattering length. For fixed L , i.e. a fixed trap size, we may consider the transition from a constant ground state to a single-peaked ground state as a function of either particle number or

scattering length. The former case corresponds to the experimental situation of adiabatic accretion of particles in pseudo-1D. The latter corresponds to the tuning of a scattering length, by a Feshbach resonance²⁵ or other means.

Thus we would expect under adiabatic growth of the condensate to observe the density of the attractive BEC, as a function of particles trapped, to be constant, then to peak in the middle, thereby breaking symmetry in an unpredictable manner, and finally to disappear from view as the width of the peak becomes less than the wavelength of the imaging radiation. In Fig. 16 we show this sequence of events in four stages superimposed on each other.

Under box boundary conditions we expect a similar occurrence. Although the ground state is not a constant, it is quite broad for $\lambda^{-1} \sim 1$. As λ^{-1} increases the ground state becomes steadily sharper until it is no longer visible under the imaging radiation. We show the prediction in Fig. 17.

Though it has been shown that the NLSE models the BEC quite well in the repulsive case, it has been unclear as to how well it models the physics of the attractive case. There have been relatively few experiments with attractive interactions, and analysis of the NLSE in a three-dimensional trapped condensate suggested a small upper limit on the number of atoms that can be maintained in a stable condensate^{1-3,6}.

We predict that in pseudo-1D, i.e. for transverse dimensions on the order of η , a slow enough accretion of particles to the attractive condensate will have the sequence shown in Fig. 16 and Fig. 17 for the ring and box, respectively. An experiment looking for such a change in the shape of the ground state could answer both questions at once: whether there are bright solitons and whether the NLSE is a useful model for the attractive BEC.

If it could be shown that the NLSE models the attractive BEC in pseudo-1D then there are a plethora of interesting phenomena in fiber optics which could have a direct analogue in the BEC.

B. Modulational instability

For $\lambda^{-1} < \sqrt{2}\pi$ we have shown that the constant solution is the ground state. We have discussed the case of adiabatic changes in the particle number or the scattering length. Let us consider now *non-adiabatic* changes.

We first note that the depth of the dn solutions is highly scale dependent. We solve Eq. (24) in the limit as $m \rightarrow 0^+$ for λ^{-1} :

$$\lambda^{-1} = \sqrt{2}\pi j \quad (51)$$

For each $j \in \{1, 2, 3, \dots\}$ there is a scale for which the real, j -peaked dn solution is in fact a constant. Near

these scales the dn solution is very shallow. Midway between them the dn solution nearly goes to zero between the peaks. We plot such an occurrence for the $j = 5$ solution dn solution over scale in Fig. 18. These solutions maintain the same phase quanta, $n = 0$, yet vary greatly in depth with only a small fluctuation of scale. This extreme sensitivity in the form of the solutions to an external parameter, here λ^{-1} , is akin to the modulational instability found in fiber optics, in which a continuous wave laser picks up highly variable sidebands in response to small changes in the power⁷.

If the scattering length is positive then the BEC is repulsive and the ground state on a ring is the constant solution. Using a Feshbach resonance the scattering length may be tuned rapidly negative. What has been seen experimentally is that the condensate simply disappears from view²⁸. There have been various explanations of this observation.

We show here that without going beyond even the stationary NLSE there is an explanation, at least in pseudo-1D. For a fast transition in the scattering length we expect the constant solution, in response to noise, to be able to easily shift to a many peaked soliton solution without having to change phase quantum number.

It may even be possible to control the form of this transition by using intentional noise to induce the desired j -peaked soliton train solution. Induced modulation has proven quite useful in fiber optics, as for example in the creation of a new kind of laser⁷.

VI. CONCLUSION

We have solved for the amplitude, phase, and chemical potentials of the complete set of solutions to the stationary nonlinear Schrödinger equation under periodic and box boundary conditions in one dimension. In a box all solutions may be taken to be real. On a ring there are four solution types: constant amplitude solutions which are plane waves; real, anti-symmetric, symmetry-breaking solutions; real, symmetric, nodeless, symmetry-breaking solutions; and intrinsically complex symmetry-breaking solutions. All of the solution types are based on Jacobian elliptic functions.

The real solutions in the box are in one-to-one correspondence with the particle-in-a-box solutions to the linear Schrödinger equation. They have two limits. The length scale of the condensate is the ratio of the healing length to the box length, λ . In the limit as $\lambda \sim 1$ the linear quantum mechanics, particle-in-a-box solutions and chemical potentials are recovered. In the limit as $\lambda \rightarrow 0^+$ the solutions become bright solitons.

The symmetry-breaking antisymmetric and constant amplitude solutions on the ring are also in one-to-one correspondence, in this case with the respective real and complex particle-on-a-ring solutions to the linear Schrödinger equation. The real solutions have a simi-

iar set of limits to the solutions in the box: as $\lambda \sim 1$ the linear quantum mechanics, real particle-on-a-ring solutions and chemical potentials are recovered, while in the limit as $\lambda \rightarrow 0^+$ the solutions become bright solitons. On a ring bright solitons come in pairs rather than singly, as they do in a box.

The real symmetric and intrinsically complex solutions on a ring, both nodeless, have no corresponding solutions in linear quantum mechanics. They take the form of stationary trains of bright solitons. As these bright solitons may be placed anywhere on the ring, they are symmetry-breaking solutions, and have a high degeneracy. Thus we may determine their entropy in analogy with vortices in two dimensions.

We have provided chemical potential spectra over experimentally reasonable scales for all solution types. We have provided plots of amplitude and phase for a sample scale of $\lambda = 1/25$.

Putting the real symmetric, the real anti-symmetric, and the complex soliton-train solution types together, we showed by group theoretic considerations that they include all symmetry-breaking eigenstates of evenly spaced peaks identical up to a phase. The total number of nearly-degenerate j -peaked solutions is j , as determined by the C_j point symmetry group. We have provided algorithms for calculating the precise splitting. For even j there is one real symmetric solution, one real anti-symmetric solution, and $(j-2)/2$ two-fold degenerate complex solutions. For odd j there is one real symmetric solution and $(j-1)/2$ two-fold degenerate complex solutions. Each of these solutions in turn has an additional degeneracy due to its breaking of symmetry.

We were able to set three kinds of bounds on the nodeless solutions on the ring: the maximum chemical potential, the minimum and maximum phase quantum number, and the minimum number of healing lengths per box length λ^{-1} needed to obtain j peaks. The bounds relied on the idea that one can only fit so many peaks on the ring before they overlap so much that they are no longer solutions to the NLSE.

Following these bounds we showed that when λ^{-1} is smaller than $\pi\sqrt{2}$ no nodeless solutions are possible, and that as λ^{-1} is increased $j = 1, 2, 3, 5, 4, 7, 9, 6, 11, 13, 8, \dots$ peaked solutions become available, in that order. In general there are many more odd j solutions than even j solutions due to the half integer nature of the lower bound of $j/2$ on the phase quantum number. This can lead to an oscillating height of the peaks as the number of them is varied.

We gave two examples of experimental predictions based on this work. The first was that as particles are adiabatically accreted onto the BEC ground state, both in the box and on the ring, gradually changes from a broad, flat distribution to a single, sharp peak. Using a fixed wavelength for the imaging radiation, the observer would see the condensate gradually peak in the middle until it disappeared from view. We suggest that an experiment along these lines would answer two questions:

is the NLSE with attractive nonlinearity a good model for the attractive BEC and, given the former, can one observe solitons in the attractive BEC?

The second prediction was that for *non-adiabatic* changes in the scattering length it is possible to transition from the constant solution to a many-peaked or clumped solution, all within the context of the NLSE. While using a Feshbach resonance to tune the scattering length from positive to negative, so that the ground state went from the constant solution to something very different, a three-dimensional BEC was observed to disappear from view. We suggest a 1D experiment be done and solutions of the type we have found be considered, in order to better understand non-adiabatic changes in the healing length, the use of a Feshbach resonance, and the associated disappearance of the condensate. It may be that the kind of fluctuations we predict, known in fiber optics as modulational instability, could be, as in fiber optics, controlled and used beneficially.

Thus far only three-dimensional experiments have been performed for the attractive BEC. The pseudo-one-dimensional solutions presented in this work may suggest further experiments.

ACKNOWLEDGMENTS

We benefited greatly from extensive discussions with Nathan Kutz and David Thouless. Early stages of this work were supported in part by the Office of Naval Research; the work was completed with the partial support of NSF Chemistry and Physics.

* to whom correspondence should be addressed

¹ C. C. Bradley, C. A. Sackett, J. J. Tollett, and R. G. Hulet, Phys. Rev. Lett., **75**, 1687 (1995).

² C. C. Bradley, C. A. Sackett, and R. G. Hulet, Phys. Rev. A, **55**, 3951 (1997).

³ C. A. Sackett, J. M. Gerton, M. Welling, and R. G. Hulet, Phys. Rev. Letts., **82**, 876 (1999).

⁴ E. P. Gross, Nuovo Cimento, **20**, 454 (1961).

⁵ L. P. Pitaevskii, Sov. Phys. JETP, **13**, 451 (1961).

⁶ R. J. Dodd, M. Edwards, C. J. Williams, C. W. Clark, M. J. Holland, P. A. Ruprecht, and K. Burnett, Phys. Rev. A, **54**, 661 (1996).

⁷ Akira Hasegawa, *Optical Solitons in Fibers* (Springer-Verlag, New York, 1990).

⁸ R. Y. Chiao, I. H. Deutsch, J. C. Garrison, and E. W. Wright in *Frontiers in Nonlinear Optics: the Serge Akhmanov Memorial Volume* 151, ed. by H. Walther, N. Koroteev, M. O. Scully (Institute of Physics Publishing, Bristol and Philadelphia, 1993).

⁹ A. V. Mamaev, M. Saffman, D. Z. Anderson, and A. A. Zozulya, Phys. Rev. A, **54**, 870 (1996).

- ¹⁰ Catherine Sulem, P. L. Sulem, *Nonlinear Schroedinger Equations: Self-Focusing Instability and Wave Collapse* (Springer-Verlag, 1999).
- ¹¹ L. D. Carr, C. W. Clark, and W. P. Reinhardt, submitted to Phys. Rev. A, (1999).
- ¹² V. E. Zakharov and A. B. Shabat, Sov. Phys. JETP, **34**, 62 (1972).
- ¹³ V. E. Zakharov and A. B. Shabat, Sov. Phys. JETP, **37**, 823 (1973).
- ¹⁴ S. A. Morgan, R. J. Ballagh, and K. Burnett, Phys. Rev. A, **55**, 4338 (1998).
- ¹⁵ W. P. Reinhardt and C. W. Clark, J. Phys. B, **30**, L785 (1997).
- ¹⁶ D. S. Rokhsar, Phys. Rev. Letts., **79**, 2164 (1997).
- ¹⁷ E. J. Mueller, P. M. Goldbart, and Yuli Lyanda-Geller, Phys. Rev. A, **57**, R1505 (1998).
- ¹⁸ Y. S. Kivshar and T. J. Alexander, cond-mat/9905048 e-print (1999).
- ¹⁹ A. D. Jackson, G. M. Kavoulakis, and C. J. Pethick, Phys. Rev. A, **58**, 2417 (1998).
- ²⁰ W. P. Reinhardt, Proceedings from the Institute for Nuclear Theory, **5**, 277 (1998).
- ²¹ M. Abramowitz and I. A. Stegun (Eds.), *Handbook of Mathematical Functions* (National Bureau of Standards, Washington D.C. 1964).
- ²² F. Bowman, *Introduction to Elliptic Functions, with Applications* (Dover, New York, 1961).
- ²³ J. M. Kosterlitz and D. J. Thouless, J. Phys. C, **6**, 1181 (1973).
- ²⁴ Y. S. Kivshar and B. Luther-Davies, Physics Reports, (1998).
- ²⁵ Y. Kagan, E. L. Surkiv, and G. V. Shlyapnikov Phys. Rev. Letts, **79**, 2604 (1997).
- ²⁶ M. Tinkham *Group Theory and Quantum Mechanics*, App. B (McGraw-Hill, New York, 1964).
- ²⁷ F. A. Cotton *Chemical Applications of Group Theory*, 3rd ed (Wiley-Interscience, New York, 1990).
- ²⁸ J. Stenger, S. Inouye, M. R. Andrews, H. -J. Miesner, D. M. Stamper-Kurn, and W. Ketterle, Phys. Rev. Letts., **82**, 2422 (1999).

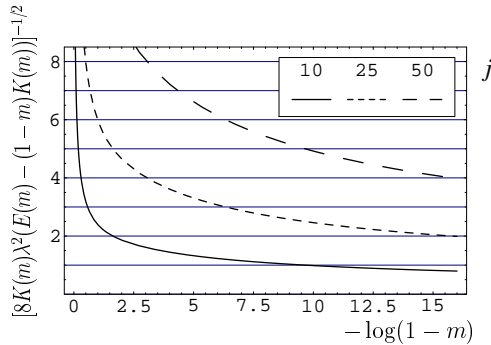


FIG. 1. This graphical solution of Eq. (7) shows that for a given scale λ^{-1} and for $j-1$ nodes the solution to the stationary NLSE in a box is unique. The three curved lines are plots of Eq. (7) solved for j , with $\lambda^{-1} = 10, 25, 50$. The left-hand side of the plot is the $m=0$, linear limit, while the right-hand side exponentially approaches the $m=1$, bright soliton limit. The solution is found where these lines intersect with the horizontal lines of j . Note the rapid convergence to $m=0$ in the high j limit, so that for large j the solutions are in the linear regime.

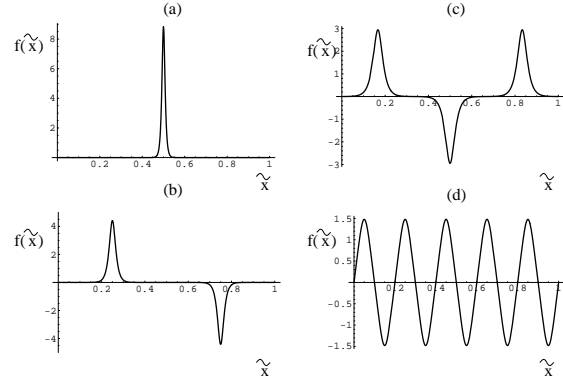


FIG. 2. Amplitude of real solutions to box boundary conditions, the NLSE analogue to the well-known particle-in-a-box problem in linear quantum mechanics. $j-1$ is the number of nodes, $\tilde{\mu}$ is the chemical potential, and all plots are for the test scale of $\xi/L = 1/25$. (a) $j=1, \tilde{\mu} = -39.0625$ (b) $j=2, \tilde{\mu} = -9.766$ (c) $j=3, \tilde{\mu} = -1.6307$ (d) a highly excited, sine-like state, $j=10, \tilde{\mu} = 0.008782$.

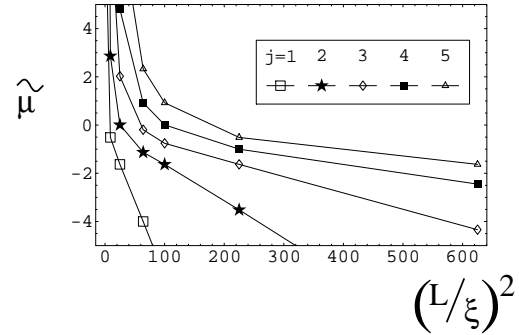


FIG. 3. Chemical potential spectrum for solutions in the box. $j-1$ is the number of nodes and (L/ξ) is the number of healing lengths per box length. These solutions are in one-to-one correspondence with the particle-on-a-ring solutions in linear quantum mechanics. The linear regime to the far right corresponds to the bright soliton limit in which the peaks are well separated, while the far left corresponds to the particle-in-a-box limit.

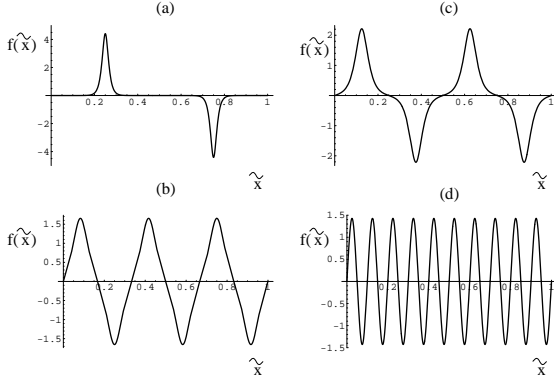


FIG. 4. Amplitude of real solutions to periodic boundary conditions, the NLSE analogue to the well-known particle-on-a-ring problem in linear quantum mechanics. $2j$ is the number of nodes, $\tilde{\mu}$ is the chemical potential, and all plots are for the test scale of $\xi/L = 1/25$. (a) ground state, $j = 1$, $\tilde{\mu} = -9.756$ (b) first excited state, $j = 2$, $\tilde{\mu} = -2.449$ (c) second excited state, $j = 3$, $\tilde{\mu} = -1.211$ (d) a highly excited, sine-like state, $j = 10$, $\tilde{\mu} = 4.801$.

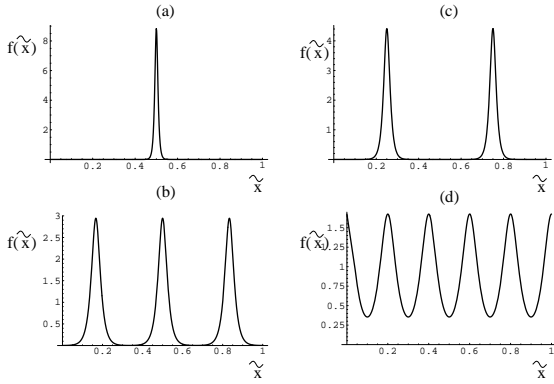


FIG. 5. Amplitude of nodeless real solutions to periodic boundary conditions, for which no analogue exists in linear quantum mechanics. j is the number of peaks, $\tilde{\mu}$ is the chemical potential, and all plots are for the test scale of $\xi/L = 1/25$. (a) ground state, $j = 1$, $\tilde{\mu} = -39.0625$ (b) first excited state, $j = 2$, $\tilde{\mu} = -9.756$ (c) second excited state, $j = 3$, $\tilde{\mu} = -4.340$ (d) the highest state at this scale, $j = 5$, $\tilde{\mu} = -1.466$.

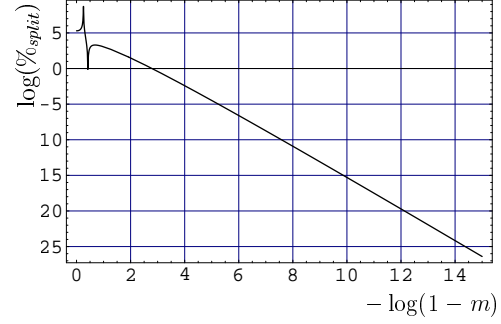


FIG. 6. Log plot of percent splitting between symmetric, nodeless dn solutions and the corresponding anti-symmetric, particle-on-a-ring type cn solutions. The left-hand side of the plot is $m \rightarrow 0^+$ while to the right m goes exponentially to 1, so that we plot the splitting where the solutions are nearly hyperbolic. Note that the symmetric solutions are *higher* in chemical potential than their corresponding anti-symmetric solutions, in contrast to intuition based on linear quantum mechanics. The noisy jag to the left is where an approximation has broken down. See Sec. IIIB 3 for details.

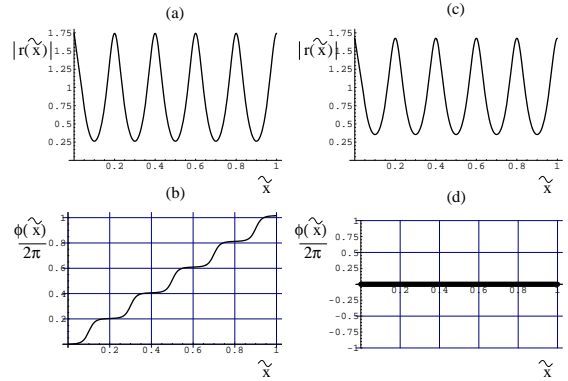


FIG. 7. Two intrinsically complex, stationary, bright soliton train solutions on a ring. j is the number of peaks, n is the phase quantum number, $\tilde{\mu}$ is the chemical potential, and all plots are for the test scale of $\xi/L = 1/25$. (a) Amplitude and (b) phase/ 2π of the $j = 5$, $n = 1$, $\tilde{\mu} = -1.5346$ solution. (c) Amplitude and (d) phase/ 2π of the $j = 5$, $n = 0$, $\tilde{\mu} = -1.4657$ solution. This latter example reproduces the five-peaked nodeless, real dn solution. Note that the former is two fold degenerate, as the chemical potential depends on n^2 .

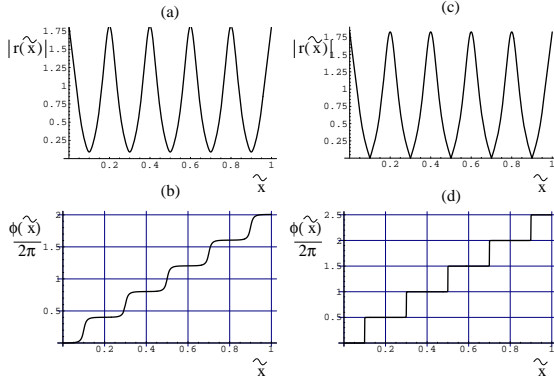


FIG. 8. An intrinsically complex, stationary, bright soliton train solution on a ring and an important limiting case of the same. j is the number of peaks, n is the phase quantum number, $\tilde{\mu}$ is the chemical potential, and all plots are for the test scale of $\xi/L = 1/25$. (a) Amplitude and (b) phase/ 2π of the $j = 5$, $n = 2$, $\tilde{\mu} = -1.6184$ solution. (c) Amplitude and (d) phase/ 2π of the $j = 5$, $n \rightarrow 2.5^-$, $\tilde{\mu} = -1.6307$ limiting case. This latter example reproduces the five-peaked cn solution in a box.

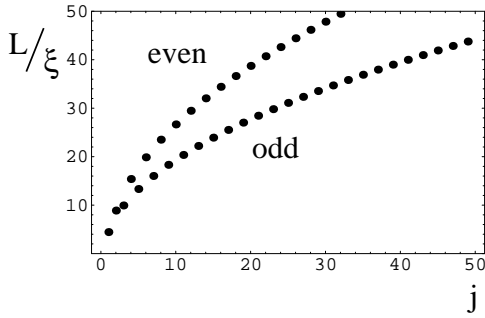


FIG. 9. Minimum inverse scale for j peaks to become available. The lower curve is odd j ; the upper curve is even j . Note that at a given inverse scale there are many more odd solutions than even solutions available. The ordering of the solutions is $j = (1, 2, 3, 5, 4, 7, 9, 6, 11, 13, \dots)$.

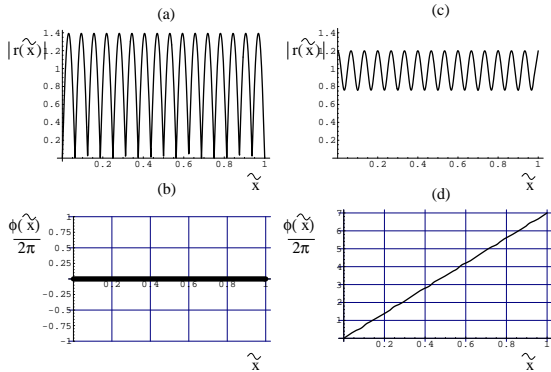


FIG. 10. Depth variation as seen in the magnitude and phase of an even and an odd-peaked solution on a ring. All plots are for the test scale of $\xi/L = 1/25$. (a) Amplitude and (b) phase/ 2π of the sixteen-peaked real cn solution. (c) Amplitude and (d) phase/ 2π of the two-fold degenerate, fifteen-peaked complex solution. In both cases these are the only solutions for this number of peaks. Note the extreme variance in depth.

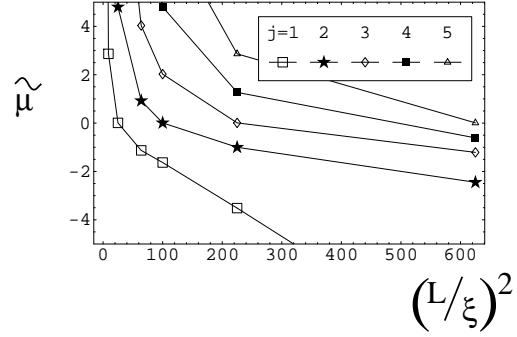


FIG. 11. Chemical potential spectrum for real, symmetry-breaking, antisymmetric solutions on the ring. $2j$ is the number of nodes and (L/ξ) is the number of healing lengths per box length. These solutions are in one-to-one correspondence with the particle-on-a-ring solutions in linear quantum mechanics. The linear regime to the far right corresponds to the bright soliton limit in which the peaks are well separated.

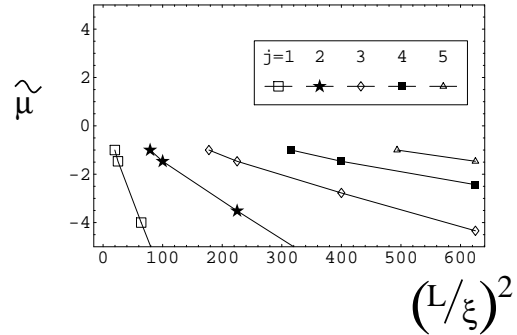


FIG. 12. Chemical potential spectrum for real, symmetry-breaking, nodeless, symmetric solutions on the ring. j is the number of peaks and (L/ξ) is the number of healing lengths per box length. These solutions have no analogue with the particle-on-a-ring solutions in linear quantum mechanics. They are nearly linear because when the peaks overlap appreciably they no longer solve the nonlinear Schrödinger equation, so that they only exist in the bright soliton regime.

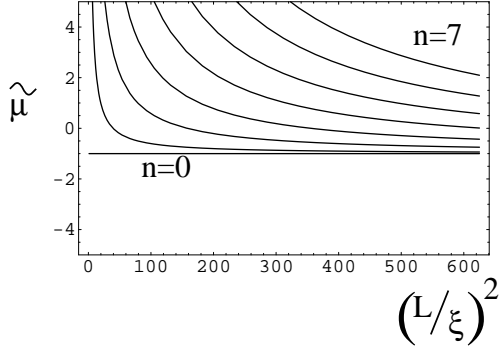


FIG. 13. Chemical potential spectrum for constant amplitude solutions on the ring. n is the phase quantum number and (L/ξ) is the number of healing lengths per box length. Curves from bottom to top are $n = 0$ to $n = 10$. These solutions are in one-to-one correspondence with the particle-on-a-ring angular momentum eigenstates in linear quantum mechanics. For $(L/\xi)^2 \leq 2\pi^2$ the $n = 0$ curve is the ground state. $n \neq 0$ curves are two-fold degenerate. These energy levels can cross with those of the other ring solution types.

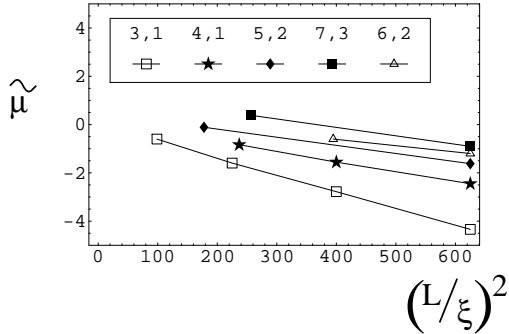


FIG. 14. Chemical potential spectrum for complex, symmetry-breaking, nodeless, symmetric solutions on the ring. j is the number of peaks, n is the phase quantum number and (L/ξ) is the number of healing lengths per box length. The labels in the legend correspond to (j, n) . These solutions have no analogue with the particle-on-a-ring solutions in linear quantum mechanics. They are nearly linear because when the peaks overlap appreciably they no longer solve the nonlinear Schrödinger equation, so that they only exist in the bright soliton regime.

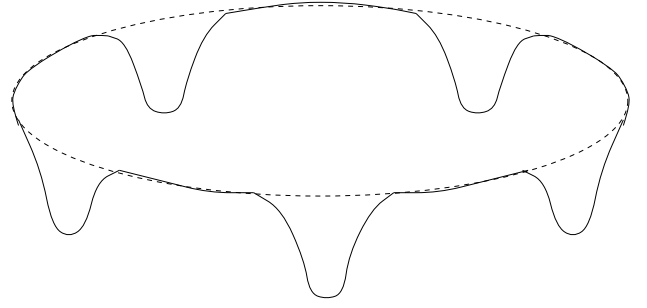


FIG. 15. Five-fold group symmetry on the ring. The dips are the mean-field effective potential produced by the five peaks in the condensate.

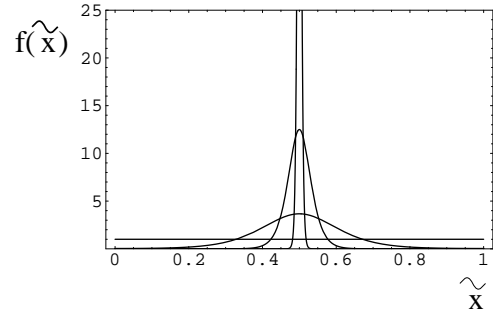


FIG. 16. Adiabatic formation of the ground state on a ring. From the broadest to the thinnest solution the scales are $L/\xi = \pi\sqrt{2}, 5, 10, 15$. The respective chemical potentials are $\tilde{\mu} = -1, -1.852, -6.250, -39.025$.

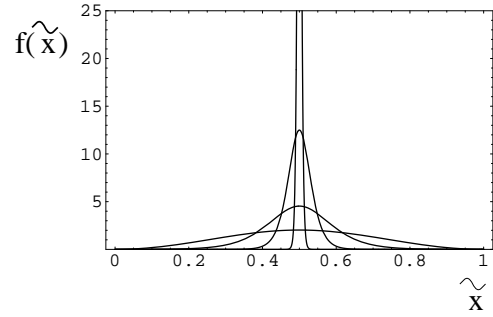


FIG. 17. Adiabatic formation of the ground state in a box. From the broadest to the thinnest solution the scales are $L/\xi = 1, 6, 10, 15$. The respective chemical potentials are $\tilde{\mu} = 8.36, -2.263, -6.250, -39.025$.

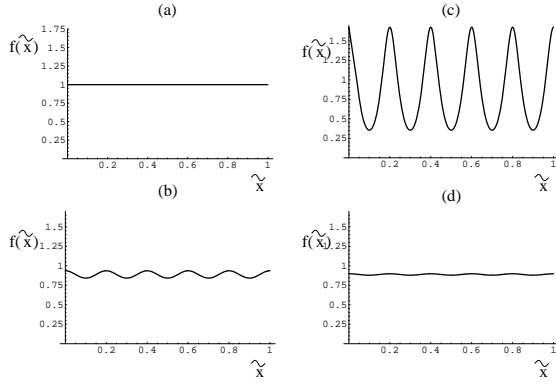


FIG. 18. Modulational instability. All four plots are for $j = 5$ peaked dn solutions, with scale varied from the minimal number of healing lengths needed to get a five-peaked solution to just less than the minimal number needed to obtain a six-peaked solution. (a) $L/\xi = 5\pi\sqrt{2}$, $\tilde{\mu} = -1.0000$ (b) $L/\xi = 22.23$, $\tilde{\mu} = -1.0028$ (c) $L/\xi = 25$, $\tilde{\mu} = -1.4657$ (d) $L/\xi = 26.658$, $\tilde{\mu} = -1.0001$